Volume 1 | Number 1 | Jan 2013 | Pages 1–100

Dalton Transactions

An international journal of inorganic chemistry
www.rsc.org/dalton

ROYAL SOCIETY OF CHEMISTRY

ROYAL SOCIETY OF CHEMISTRY

www.rsc.org/dalton

Ethylene oligomerization studies by nickel(II) complexes chelated by (amino)pyridine ligands: Experimental and density functional theory studies

George S. Nyamato, Stephen O. Ojwach* and Matthew P. Akerman

School of Chemistry and Physics, University of KwaZulu-Natal, Scottsville, South Africa

Abstract

Reductions of imine compounds 2-methoxy-N-(1-(pyridin-2-yl)ethylidene)ethanamine (**L1**), 2-methoxy-N-((pyridin-2-yl)methylene)ethanamine (**L2**), N,N-diethyl-N-((pyridin-2-yl)methylene)ethane-1,2-diamine (**L3**) and 2-((pyridin-2-yl)methyleneamino)ethanol (**L4**) using NABH$_4$ produced their corresponding amine analogues N-(2-methoxyethyl)-1-(pyridin-2-yl)ethanamine (**L1a**), 2-methoxy-N-((pyridin-2-yl)methyl)-ethanamine (**L2a**), N,N-diethyl-N-((pyridin-2-yl)methyl)ethane-1,2-diamine (**L3a**) and 2-((pyridin-2-yl)methylamino)ethanol (**L4a**) in good yields. Reactions of the (amino)pyridine ligands **L1a-L4a** with [NiBr$_2$(DME)] afforded nickel(II) complexes, [NiBr$_2$(**L1a**)$_2$] (**1**), [NiBr$_2$(**L2a**)$_2$] (**2**), [NiBr$_2$(**L3a**)$_2$] (**3**) and [NiBr$_2$(**L4a**)$_2$] (**4**), respectively in quantitative yields. Molecular structures of complexes **2** and **4** confirmed the formation of the bis(chelated)nickel(II) complexes. Activation of complexes **1-4** with either EtAlCl$_2$ or methylaluminoxane (MAO), produced active ethylene oligomerization catalysts to afford mostly ethylene dimers (C$_4$), in addition to trimmers (C$_6$) and tetramers (C$_8$). Density functional theory studies provided valuable insight into the reactivity trends and influence of complex structure on the ethylene oligomerization reactions.

Keywords: nickel(II) complex, ethylene, oligomerization, co-catalyst, DFT studies

*Corresponding author: Tel.: +27 (33) 260 5239; Fax: +27 (33) 260 5009

E-mail: ojwach@ukzn.ac.za (S. O. Ojwach)

Introduction

Oligomerization of ethylene currently constitutes one of the predominant industrial processes for the production of linear α-olefins (LAO), which are extensively used in the manufacture of a wide range of products such as oxo-alcohols used in detergents and plasticizers, poly-α-olefins for the synthetic lubricant pool, oil field chemicals and as comonomers for the production of linear low-density polyethylene (LLDPE).[1] The global supply of LAO is dominated by the ''*full-range processes*'' of Chevron Phillips Chemical (CPChem), INEOS and Shell.[2] In recent years, significant progress has been made in selective oligomerization of ethylene, targeting a narrow product distribution.[3] The quest for selective oligomerization of ethylene has been driven by the souring demand for C_4-C_{10} olefins for the production of linear low-density polyethylene resins (LLDPE).[4]

Originally, LAOs were manufactured by the Ziegler (Alfen) process[5] while the current industrial processes utilize catalysts that include either alkylaluminium and early or late transition metal complexes[6, 7] In the past decade, transition-metal catalyzed ethylene oligomerization of ethylene to short chain α-olefins has attracted great attention in both academic and industrial research.[8, 9] When compared to conventional catalysts, late-transition metal catalysts have the advantage of being less electrophilic and better tolerant to polar monomers.[10]

The discovery of α-diimine-type nickel(II) complexes by Brookhart and co-workers[11-13] as highly active pre-catalysts for ethylene oligomerization and polymerization, has revitalized research into nickel(II) systems for ethylene reactivity. To date, the major focus has fundamentally been on ligand design and the insights gained so far indicate that the ability to control the catalytic behavior of any catalyst lies in the coordination environment which can be systematically varied by changing the ligand motif.[14-16] Unfortunately, despite extensive

research, the influence of ligand environment on catalytic properties of a transition metal complex still remains a major challenge to predict.[16-18]
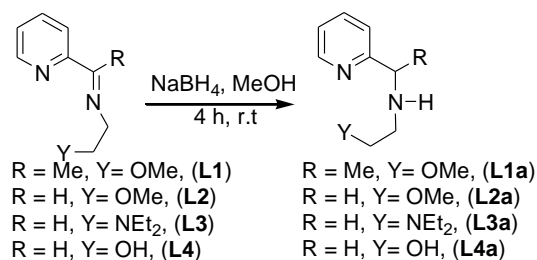
In this study, we report the use of (imino)pyridine ligands to make nickel(II) complexes as potential catalysts in olefin oligomerization reactions. Attempts to use the imine ligands (**L1**-**L4**) we previously used to prepare palladium complexes[19] to synthesize nickel(II) complexes did not materialize. This could have been largely due to hydrolysis of the imine group in the ligands as reported in literature.[20, 21] To circumvent this drawback, the imine ligands (**L1**-**L4**) were reduced to their analogous amines and subsequently used to prepare new (amino)pyridine nickel(II) complexes. Thus herein, we report the syntheses and structural characterization of these (amino)pyridine nickel(II) complexes and their behavior as ethylene oligomerization pre-catalysts. Further theoretical studies using density functional theory has been performed to shed more light on the effect of complex structure on the catalytic behavior of these catalysts in ethylene oligomerization reactions.

Results and discussion

Syntheses of (amino)pyridine ligands and their complexes

Treatment of the (imino)pyridine ligands 2-methoxy-N-(1-(pyridin-2-yl)ethylidene)ethanamine (**L1**)**,** 2-methoxy-N-((pyridin-2-yl)methylene)ethanamine (**L2**)**,** N,N-diethyl-N-((pyridin-2-yl)methylene)ethane-1,2-diamine (**L3**) and 2-((pyridin-2-yl)methyleneamino)ethanol (**L4**) with excess amounts of NABH$_4$ produced the respective (amino)pyridine ligands N-(2-methoxyethyl)-1-(pyridin-2-yl)ethanamine (**L1a**), 2-methoxy-N-((pyridin-2-yl)methyl)-ethanamine (**L2a**), N,N-diethyl-N-((pyridin-2-yl)methyl)ethane-1,2-

diamine (**L3a**) and 2-((pyridin-2-yl)methylamino)ethanol (**L4a**) in quantitative yields (Scheme 1).

R = Me, Y= OMe, (**L1**)   R = Me, Y= OMe, (**L1a**)
R = H, Y= OMe, (**L2**)   R = H, Y= OMe, (**L2a**)
R = H, Y= NEt₂, (**L3**)   R = H, Y= NEt₂, (**L3a**)
R = H, Y= OH, (**L4**)   R = H, Y= OH, (**L4a**)

Scheme 1: Synthesis of (amino)pyridine ligands *via* reduction of their respective imine compounds

The ligands were characterized by ^{1}H NMR, ^{13}C{^{1}H} NMR and FT-IR spectroscopy, mass spectrometry and elemental analyses. ^{1}H NMR spectra of the ligands showed signature peaks expected for the amine compounds in relation to the imine analogues. For example, the emergence of new singlets between 3.88-3.93 ppm attributed to CH_2 protons in **L1a**-**L4a** in addition to the absence of the imine signal between 8.31-8.45 ppm confirmed successful reduction of the imine ligands to their corresponding amine compounds **L1a**-**L4a** (Fig. S1). In the ^{13}C-NMR spectra of **L2a**, a signature carbon peak of the –CH_2- group was recorded up-field at 54.7ppm compared to 163.5 ppm of the imine carbon in **L2** (Fig. S2). IR stretching frequencies between 3278 and 3366 cm^{-1} reported for **L1a**-**L4a** were indicative of the formation of secondary amines.[22] Further analyses by mass spectrometry of **L1a-L4a** produced molecular ions associated with the formulae depicted in Scheme 1. Elemental analyses data of all the compounds were in agreement with the proposed empirical formulae and confirmed their purity.

Reactions of the (amino)pyridine ligands **L1a-L4a** with one equiv. of [NiBr₂(DME)] (Scheme 2) led to the formation of bis(chelated)nickel(II) complexes **1-4**, in good yields (75-

4

83%). Complex **1** was obtained as a brown solid, complexes **2** and **3** as green solids, while complex **4** was obtained as a violet solid.
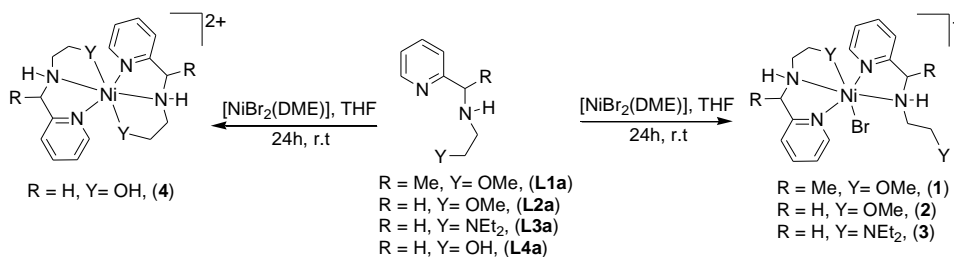
Scheme 2: Synthesis of (amino)pyridine nickel(II) complexes. The bromide counter anions are omitted.

Due to the paramagnetic nature of complexes **1**-**4**, NMR spectroscopy was not useful in their structural characterization. The complexes were thus characterized by magnetic moment measurements, elemental analyses, mass spectrometry and single crystal X-ray analysis for **2** and **4**. The magnetic moments of the nickel(II) complexes **1**-**4** were recorded between 3.70-3.77 BM. These values were effectively higher than the predicted spin only value of 2.83 BM for nickel(II) complexes, but fall within the expected range for high spin nickel(II) complexes of 2.9-4.2 BM[23] when spin orbital contribution is considered.

Mass spectrometry data for all the complexes showed molecular fragmentation patterns consistent with the formation of bis(chelated)nickel(II) complexes. It is interesting to note that complexes **1**-**3** showed base peaks containing only one ligand unit. For example, complex **2** showed a base peak at m/z = 304 corresponding to one ligand unit in the complex (Fig. S3). However, the base peak for complex **4** (m/z = 361) correlates to the bis(chelate)nickel(II) complex (Fig. S4). Thus mass spectral data of all the complexes (except for **4**) point to possible dissociation of one ligand unit to form the mono(chelated)nickel(II) species. The relative stability of complex **4** possibly due to the stronger binding affinity of Ni to OH[24] may account

for the observed bis(chelated) species. The formation of the bis(chelated)nickel(II) complexes was unambiguously proved by the crystal structures of complexes **2** and **4** (Figs. 1 and 2). Elemental analyses data of complexes **1**-**4** were consistent with the presence of two ligand units per nickel(II) metal as proposed in Scheme 2.

Molecular structures of complexes 2 and 4

The solid state structure of compound **2** shows that it is a bis(pyridyl-amine) chelate. Interestingly, the coordination mode of each ligand is not equivalent. The first acts as a tridentate ligand with coordination to the nickel(II) ion through the pyridyl and secondary amine nitrogen as well as the methoxy oxygen atom. The second ligand coordinates in a bidentate manner through the pyridyl and amine nitrogen atoms only. The sixth coordination site is occupied by a bromide ligand, yielding a nominally octahedral coordination geometry. Both the secondary amines coordinated the metal ion without concomitant deprotonation; the chelate is therefore a mono-cationic bromide complex salt. The asymmetric unit of compound **2** is shown in Fig. 1. The hydrogen bonding potential of the amine NH groups does not lead to an extended supramolecular structure; both showing direct hydrogen bonding to the bromide counter ion.
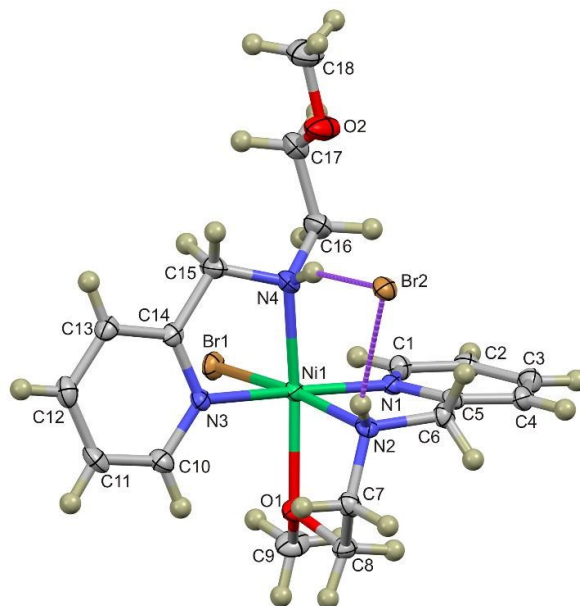
Fig. 1: Asymmetric unit of compound **2** with thermal ellipsoids rendered at the 50% probability level. Hydrogen bonds between the two amine N–H groups and bromide ion are indicated as broken purple tubes.

Compound **4** shows an octahedral nickel(II) centre with two tridentate ligands coordinated. The secondary amine and hydroxyl units both coordinate without deprotonation. The molecule possesses crystallographically imposed inversion symmetry and crystallises in the triclinic space group *P*–1 with a single molecule in the unit cell. The asymmetric unit of compound **4** comprises a half nickel(II) ion located on an inversion centre with a single (neutral) tridentate ligand coordinated and a single full site occupancy bromide ion and water molecule. The bond parameters describing the octahedral coordination spheres of compounds **2** and **4** are summarised in Table 2 and clearly indicate the nominally octahedral geometry of both structures. The bond parameters show that the small bite angle of the ligands, which yield a five-membered chelation ring, are more acute than the ideal angle. Correspondingly, the bond angles which are not constrained by the ligand geometry are more obtuse.
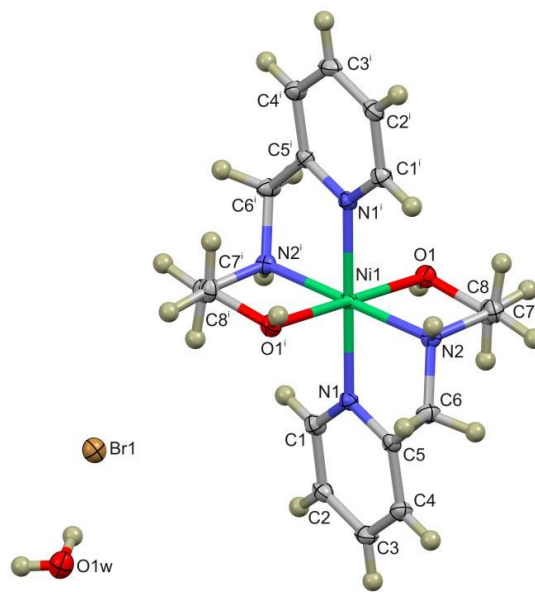
Fig. 2: Symmetry-completed solid state structure of compound **4** with thermal ellipsoids rendered at the 50% probability level.

The solid state structure of compound **4** exhibits several hydrogen bonds. The bromide ion acts as an H-bond acceptor for three hydrogen bonds between the amine NH and two hydrogen atoms of the water molecule. Additionally, the water molecule acts as an H-bond acceptor for the ligand O–H moiety. The result of this hydrogen bonding pattern is an infinite one-dimensional chain with adjacent metal cations bridged by two water molecules and two bromide ions, as shown in Fig. S5. The hydrogen bond parameters are summarised in Table S1. Although the bond lengths do not necessarily correlate linearly with bond strength due to packing constraints in the lattice, the hydrogen bonds exhibited by both structure **2** and **4** are significantly shorter than the sum of the van der Waals radii. This, coupled with the fact that hydrogen bond lengths particularly those of compound **4** approach the ideal, suggests that the interactions are likely to be moderately strong.[25]

8

Table 1: Crystal data and structure refinement for complexes **2** and **4**

Parameter	2	4
Empirical formula	$C_{18}H_{26}Br_2N_4NiO_2$	$C_{16}H_{24}N_4NiO_2 \cdot 2(Br) \cdot 2(H_2O)$
Formula weight	550.97	558.91
Temperature(K)	100(2) K	100(2) K
Wavelength (Å)	0.71073 Å	0.71073 Å
Crystal system	Triclinic	Triclinic
Space group	P-1	P-1
a, b, c (Å)	9.2476(5), 9.8870(6), 12.5210(7)	8.1950(4), 8.3725(4), 8.9081(4)
α, β, γ (°)	92.876(3), 90.579(3), 110.439(4)	109.596(2), 98.327(2), 101.729(2)°
Volume (Å^3)	1070.92(11)	548.55(5)
Z	2	1
Crystal size (mm)	$0.19 \times 0.11 \times 0.04$	$0.19 \times 0.08 \times 004$
Density (calculated) (Mg/m^3)	1.709	1.692
Absorption coefficient (mm^{-1})	4.66	4.55
F(000)	556	282
Number of reflections	4168	2119
Goodness-of-fit on F^2	1.13	1.09
R indices (all data)	$R_1 = 0.033$	$R_1 = 0.024$
	$wR_2 = 0.084$	$wR_2 = 0.063$
Largest diff. peak and hole (e.Å^{-3})	0.91 and -0.97	0.63 and -0.59

Table 2: Summary of the bond lengths (Å) and bond angles (°) describing the coordination spheres of compounds **2** and **4**.

2				4			
Bond lengths [Å]		**Angles [º]**		**Bond lengths [Å]**		**Angles [º]**	
Ni1–Br1	2.5394(5)	Br1–Ni1–N1	95.11(8)	Ni1–O1	2.116(2)	N1–Ni1–N2	81.29(7)
Ni1–O1	2.200(2)	N1–Ni1–N2	81.1(1)	Ni1–N1	2.079(3)	N1–Ni1–N2^i	98.71(8)
Ni1–N1	2.071(3)	N2–Ni1–N3	95.3(1)	Ni1–N2	2.081(3)	O1–Ni1–O1^i	180.0
Ni1–N2	2.112(2)	N3–Ni1–Br1	88.53(8)				
Ni1–N3	2.078(3)	N3–Ni–N4	81.01(1)				
Ni1–N4	2.106(3)	O1–Ni1–N4	169.2(1)				

Symmetry code: (i) –x, –y, –z

Ethylene oligomerization reactions catalyzed by complexes 1-4

*Preliminary evaluation of complexes **1**-**4** as catalysts in ethylene oligomerization reactions*

Nickel(II) complexes **1**-**4** were evaluated as pre-catalysts in the oligomerization of ethylene using ethylaluminium dichloride (EtAlCl$_2$) and methylaluminoxane (MAO) as co-catalysts. In both cases, the complexes formed active catalysts in ethylene oligomerization reactions to produce predominantly butenes and some small amounts of hexenes and octenes (Table 3). The identities of these oligomerization products were established by a combination of GC and GC-MS (Figs. S6-S10).

Table 3: Ethylene oligomerization data for **1**-**4** catalytic systems.[a]

Entry	Catalyst	Cocat.	Al:M	Yield (g)	Activity[b]	%Oligomer distribution[c]				
						C_4	C_6	C_8	α-C_4	α-C_6
1	**1**	EtAlCl$_2$	200	10.8	2 160	64	32	4	80	55
2	**2**	EtAlCl$_2$	200	11.9	2 380	61	35	4	72	52
3	**3**	EtAlCl$_2$	200	13.7	2 740	47	44	9	86	56
4	**4**	EtAlCl$_2$	200	9.3	1 860	54	40	6	75	52
5	**1**	MAO	1 000	9.4	1 880	77	15	8	94	56
6	**2**	MAO	1 000	8.5	1 700	74	16	10	88	51
7	**3**	MAO	1 000	11.2	2 240	71	18	11	91	58
8	**4**	MAO	1 000	9.8	1 960	72	18	10	86	56

[a]Reaction conditions: 5 μmol Ni; solvent, toluene, 80 mL; Pressure, 10 bar; Time, 1 h; temperature, 30 °C. [b]In kg oligomer. mol.Ni^{-1}.h^{-1} [c]Determined by GC.

The observed product distribution by complexes **1**-**4** is similar to those recently reported by Braunstein and co-workers using nickel(II) complexes chelated by bis(diphenylphosphino)(*N*-thioether)amine-type ligands.[26] In another study, Flapper *et al.*[27] observed the formation of mainly C_4, and small amounts of C_6 and C_8 oligomers using nickel(II) complexes bearing pyridine-phosphine ligands and MAO as a co-catalyst. In contrast to our earlier findings, complexes **1**-**4** catalyzed ethylene oligomerization reactions using $EtAlCl_2$ co-catalyst to afford mainly butenes and hexenes without subsequent Friedel-Crafts alkylation of the pre-formed oligomers by toluene solvent.[28-32] Thus it is clear that ligand moiety in the catalyst systems plays a crucial role in regulating the oligomer distribution in ethylene oligomerization reactions.

The observed catalytic of complexes **1**-**4** of 1 860-2 740 kg oligomer.mol.$Ni^{-1}.h^{-1}$ are comparable to those previously reported for nickel(II) of 2-(1-aryliminoethylidene)quinolyl ligands of 478-2 760 kg oligomer.mol.$Ni^{-1}.h^{-1}$.[33] However, the activities reported for **1**-**4** were several orders of magnitudes lower than those obtained by Chavez *et al.*[34] of 79×10^3 h^{-1} to 230×10^3 h^{-1} using nickel(II) phoshinito-oxazoline complexes. It is important to note that while both systems reported by Song *et al.* and Chavez *et al.* produce exclusively butenes, catalysts **1**-**4** produced mostly butenes in addition to small amounts of hexenes and octenes.

*Effect of co-catalyst on ethylene oligomerization reactions by **1**-**4***

In general, all the complexes exhibited higher catalytic activities upon activation using $EtAlCl_2$ compared to when MAO was used as the co-catalyst. For example, catalytic activities of up to 2 740 kg oligomer.mol.$Ni^{-1}.h^{-1}$ and 2 240 kg oligomer.mol.$Ni^{-1}.h^{-1}$ were obtained using $EtAlCl_2$ and MAO co-catalysts respectively. The observed differences in catalytic activities with the nature of the co-catalyst may be attributed to the different nature of the active species formed

during the activation process.[35, 36] In this present case, it is believed that coordination of the Al

metal in the co-catalyst to the pendant donor atoms might lead to enhanced catalytic activities, as

has been reported by Barzan and co-workers.[37, 38]

The nature of the co-catalyst was also noted to affect product distribution. For example,

activation using MAO displayed higher selectivities towards butenes (71%-77%) compared to

EtAlCl$_2$ (47% to 64%). Moreover, the use of MAO gave higher selectivities for 1-butene (86%-94%)

compared to EtAlCl$_2$ (72% to 86%). Thus, activation using EtAlCl$_2$ favored formation of hexenes

compared to MAO. Change in product distribution due to the nature of co-catalyst has also been

previously reported for ethylene oligomerization reactions using nickel(II) complexes.[39-41]

Influence of catalyst structure on ethylene oligomerization reactions

The effect of complex structure on the catalytic activities of **1-4** was investigated for both

EtAlCl$_2$ and MAO co-catalysts (Table 3). It is evident that the ligand environment influenced the

catalytic performance of these nickel(II) complexes (**1-4**). For example, complex **1**, containing a

methyl substituent exhibited lower catalytic activity of 2 160 kg oligomer mol.Ni^{-1}.h^{-1}, compared to

the unsubstituted complex **2** (2 380 kg oligomer.mol.Ni^{-1}.h^{-1}), Table 3, entries 1 and 2. Thus the

electron donating ability of the methyl group in **1** is likely to decrease the net positive charge on the

nickel(II) atom, resulting in diminished ethylene coordination.[42-44] The nature of the pendant donor

group was also noted to influence the catalytic activities of the complexes. As an illustration,

substitution of a methoxy group in **2** by an amino group (**3**) led to increased catalytic activities from 2

380 kg oligomer.mol.Ni^{-1}.h^{-1} to 2 740 kg oligomer.mol.Ni^{-1}.h^{-1} respectively. This is consistent with

similar findings on nickel(II) complexes chelated by imino-imidazole ligands in which substitution of

an ether group by an amino group resulted in improved catalytic activity.[45] Stronger coordination of

13

O atom to Ni (hard-soft acid base theory)[24] may result in competition with the incoming ethylene monomer for the vacant coordination site. It is therefore not surprising that complex **4**, bearing the OH group, showed the lowest catalytic activity.

*Effect of reaction conditions on ethylene oligomerization behavior of pre-catalyst **2***

The effect of reaction parameters such as co-catalyst concentration, pressure and time were investigated using complex **2** and EtAlCl$_2$ as co-catalyst (Table 4). First, we varied the Al/Ni ratio from 100 to 300. An increase in Al/Ni ratio from 100 to 200 was marked by a concomitant increase in catalytic activity from 1 460 kg oligomer.mol.Ni^{-1}.h^{-1} to 2 380 kg oligomer.mol.Ni^{-1}.h^{-1} (Table 4, entries 1 and 2). However, a further increase of the Al/Ni ratio to 300 led to a reduction in catalytic activity to 2 680 kg oligomer.mol.Ni^{-1}.h.$^{-1}$ Reduction of catalytic activity with higher Al/Ni ratios has been largely associated with possible deactivation from build-up in impurities and ash/alumina content.[32] Variation of Al/Ni ratio also had an effect on the oligomer distribution. For instance, increasing the Al/Ni ratio from 100 to 300 resulted in a marginal decrease in C$_4$ selectivity from 65% to 57%, respectively, accompanied by a slight increase in the composition of hexenes from 31% to 38%. Moreover, it was observed that increasing the Al/Ni molar ratio from 100 to 300 (Table 4, entries 1−4) resulted in increased selectivity for 1-butene from 71% to 82%. Similar trends on α-olefin selectivity with increasing Al/Ni ratio has been previously reported.[46-48]

Table 4: Ethylene oligomerization data for **2** using EtAlCl$_2$ as co-catalyst in toluene.[a]

Entry	Catalyst	Pressure (bar)	Time (h)	Al:Ni	Yield (g)	Activity[b]	%Oligomer distribution[c]				
							C$_4$	**C$_6$**	**C$_8$**	**α-C$_4$**	**α-C$_6$**
1	**2**	10	0.5	200	3.9	1 560	66	30	4	74	47
2	**2**	10	1	200	11.9	2 380	61	35	4	72	52
3	**2**	10	2	200	19.2	1 920	56	39	5	73	51
4	**2**	10	1	100	7.3	1 460	65	31	4	71	50
5	**2**	10	1	250	16.6	3 320	58	37	5	79	47
6	**2**	10	1	300	13.4	2 680	57	38	5	82	51
7	**2**	5	1	200	6.5	1 300	58	37	5	69	54
8	**2**	20	1	200	16.7	3 340	64	33	3	78	53
9	**2**	30	1	200	21.1	4220	69	28	3	87	57
10[d]	**2**	10	1	200	21.5	4300	77	17	6	54	52
11[d]	**4**	10	1	200	17.3	3460	73	16	11	52	48

[a]Reaction conditions: 5 μmol Ni; solvent, toluene, 80 mL; temperature, 30 °C; Time, 1 h. [b]In kg oligomer.mol.Ni^{-1}.h^{-}
[1c]Determined by GC. [d]Solvent, chlorobenzene.

As expected, increase in ethylene pressure led to higher catalytic activities. For example, activities of 1 300 kg oligomer.mol.Ni^{-1}.h^{-1} and 4 220 kg oligomer.mol.Ni^{-1}.h^{-1} were realized at 5 bar and 30 bar, respectively (Table 4, entries 7 and 9). This trend has been attributed to increased ethylene concentration in solution.[30, 49] We also observed increased composition of butenes from 58% to 69% with increase in pressure from 5 bar to 30 bar, respectively (Table 4, entries 7and 9) as well as higher selectivity for 1-butene. Greater selectivity for α-olefins at higher pressures has been ascribed to rapid chain transfer relative to chain isomerization.[50-52] Consistent with earlier reports,[21, 30, 32] reactions conducted in chlorobenzene solvent showed higher catalytic activities compared to those performed in toluene (Table 4, entries 2 and 10).
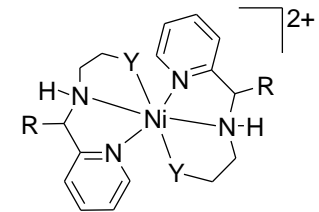
Catalyst stability is a fundamental factor for feasible industrial considerations. Thus, we probed the relative stabilities of complexes **2** and **4**, by varying reaction times between 0.5 h to 2 h (Table 4 and Fig S11). For complex **2**, we observed an initial increase in catalytic activity from 1 560 kg oligomer mol.Ni^{-1}.h^{-1} to 2 380 kg oligomer.mol.Ni^{-1}.h^{-1} between 0.5 h and 1 h, respectively. However, increasing the reaction time to 2 h resulted in decreased catalytic activity to 1 920 kg oligomer.mol.Ni^{-1}.h^{-1} (Table 4, entries 1-3). These two processes could be associated with activation of the pre-catalyst between 0.5 h to 1 h, followed by subsequent deactivation. From the relative drops in catalytic activities, it is evident that the more active catalyst **2** displayed lower stability than the less active catalyst **4** (Figure S11). It was also observed that longer reaction times resulted in a slight decline of the selectivity for butenes, varying from 66% (0.5 h) to 56% (2 h), but did not have a significant impact on the selectivity for α-olefins. Furthermore, a slight increase in the amount of C$_6$ from 30% (0.5 h) to 39% (2 h) was noted, which may be attributed to olefin reincorporation over longer reaction times.[53]

Density functional theoretical calculations of reactivity parameters for complexes 1-4

In order to gain insight into the catalytic trends of complexes **1**-**4**, DFT studies were performed using a split basis set LANL2DZ for nickel(II) and 6311G(dp) for the remaining atoms. The experimental data from the molecular structures of bis(chelated) complexes **2** and **4** (Figs. 1 and 2) were used to validate the data from the calculated geometries. Table S2 shows selected bond lengths while Table 5 shows the positive net charges of the nickel(II) metal centers of complexes **1**-**4**, Ni-Y (pendant donor atom) bond lengths, as well as the HOMO-LUMO energy gaps ($\Delta\varepsilon$) between the complexes and ethylene. The HOMO-LUMO energy gaps ($\Delta\varepsilon$) [kcal/mol] were determined from the energy differences between the pre-catalysts' LUMO and ethylene's HOMO. The atomic coordinates of the calculated structures are given as supplementary information.

From Table S2, it is evident that the calculated bond lengths were comparable to the experimental values obtained by X-ray crystallography, except for the Ni-O bonds that were longer than the experimental values of complexes **2** and **4**, probably due to steric crowding around the metal center. Nonetheless, from both the experimental and theoretical data, the average Ni-O bond length in complex **4** was shorter compared to the Ni-O bond length in complex **2**, indicating strong coordination of OH than OCH$_3$ group to nickel(II) atom.

Table 5: Theoretical and experimental data for complexes **1-4**

Complex	NBO charge (Ni)	Δε [kcal/mol]	Ni-Y (Å)	Activity[a]	
1	1.201	83.10	2.6261	2 160	
2	1.210	85.18	2.6529	2 380	R = Me, Y= OMe, (**1**)
3	1.242	84.69	2.8471	2 740	R = H, Y= OMe, (**2**)
4	1.191	77.78	2.5336	1 860	R = H, Y= NEt₂, (**3**) R = H, Y= OH, (**4**)

[a]In units of kg oligomer.mol.Ni^{-1}.h^{-1}

In order to delineate the dependence of the catalytic activity on the average Ni-Y (pendant donor atom) bond length, a plot of Ni-Y bond length *vs* catalytic activity was constructed (Fig. 3). It was observed that a general increase in Pd-Y bond length was followed by an increase in catalytic activity (Table 5and Fig. 3). For example, shorter Pd-O bond length of 2.5336 Å in (**4**) compared to Pd-N bond length of 2.8471 Å in **3** resulted in catalytic activities of 1 860 to 2 740 kg oligomer. mol.Ni^{-1}.h^{-1} respectively. This trend could be assigned to the ease of displacement of the pendant N(Et)₂ group prior to coordination of the incoming ethylene monomer. It is therefore conceivable that ethylene coordination to the vacant Ni(II) atom in the active species may be presumed to be the rate determining step in these ethylene oligomerization reactions.
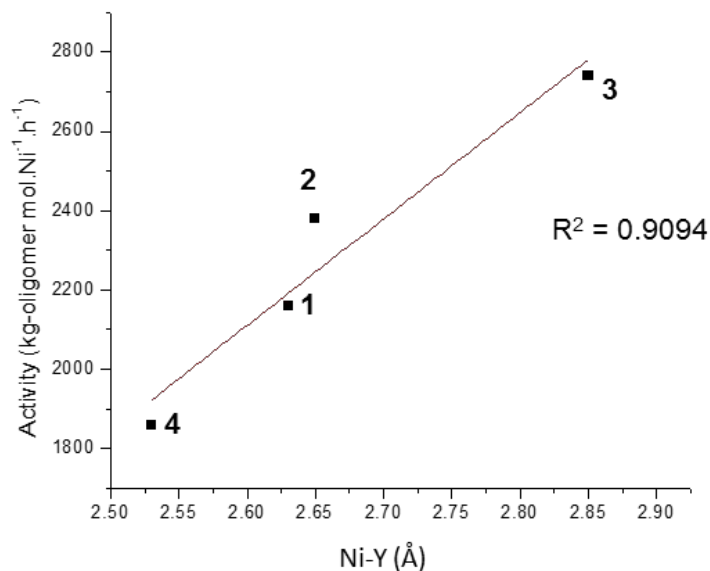
Fig. 3: Plot of activity in kg-oligomer mol.$Ni^{-1}.h^{-1}$ against Ni-Y (Å) depicting a correlation between catalytic activities and Ni-Y bond lengths.

A linear relationship between the NBO charges of the nickel(II) metal center and catalytic activity was also obtained (Fig. 4). Generally, the catalytic activities increased with higher net charge on the nickel(II) atom which could be attributed to enhanced rate of ethylene coordination to the nickel(II) center. Indeed complex **3**, carrying the greatest NBO charge of 1.240, recorded the highest catalytic activity of 2 740 kg oligomer.mol.$Ni^{-1}.h.^{-1}$ consistent with recent reports on benzylidenequinoline nickel(II) catalysts.[54]
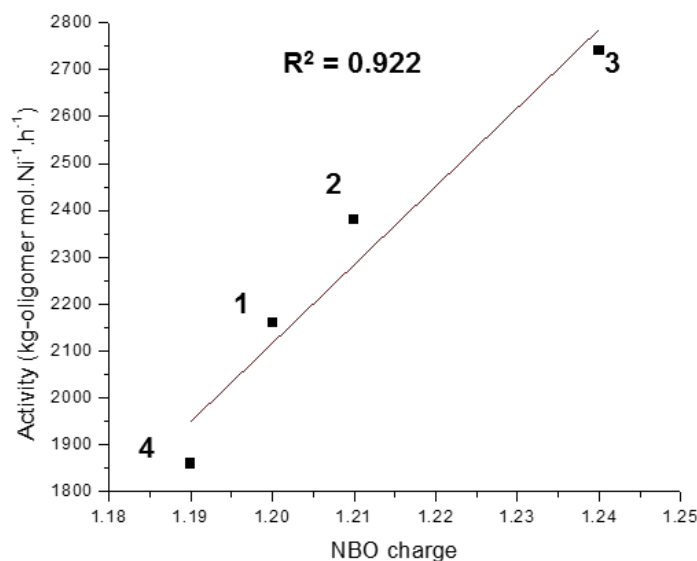
19

Fig. 4: Plot of activity (kg-oligomer mol.Ni^{-1}.h^{-1}) against NBO charge illustrating the influence of NBO charge on catalytic activity.

The HOMO-LUMO energy gaps were also investigated to study their influence on the catalytic activities of the respective complexes (Table 5). The energy differences between pre-catalysts **1**-**4**'s LUMO and ethylene's HOMO were lower than the energy differences between pre-catalysts **1**-**4**'s HOMO and ethylene's LUMO. This agrees with ethylene oligomerization reaction being a nucleophilic attack of the metal center by the ethylene monomer.[54] Thus, a smaller energy difference between HOMO and LUMO should promote coordination of ethylene substrate to the metal center. From Table 5 and Fig. S12, it is evident that the HOMO-LUMO energy gaps did not have a profound effect on the resultant catalytic activities of the complexes due to the weak correlation (R^2 = 0.568) observed. Moreover, the trend recorded contradicts the expected behaviour[55] since the catalytic activities increased with higher energy gaps ($\Delta\varepsilon$). However, this observation is consistent with a recent reports.[54] Thus, from the DFT results, it is

evident that the ethylene oligomerization reactions are charged controlled rather than a frontier-directed between the cationic nickel(II) metal centres and ethylene monomer.

Conclusions

A series of nickel(II) complexes containing (amino)pyridine ligands with pendant donor groups have been synthesized and structurally characterized. Single crystal X-ray diffraction studies of complexes **2** and **4** confirmed tridentate coordination mode of the ligands and formation of bis(chelated)nickel(II) compounds. Complexes **1**-**4** formed active catalysts for ethylene oligomerization in the presence of EtAlCl$_2$ and MAO as co-catalysts to afford mainly butenes and small amounts of hexenes and octenes. Theoretical calculations showed a correlation between catalytic activities of complexes **1**-**4** and the nature of ligand motif. Coordination of the ethylene monomer to the electrophilic nickel(II) atom is likely to be the rate determining step in these oligomerization reactions.

Experimental section

Materials and methods

All synthetic manipulations were performed using standard Schlenk techniques under a nitrogen atmosphere. All solvents were dried by distillation prior to use. Nickel(II) bromide-1,2-dimethoxyethane complex [NiBr$_2$(DME)], sodium borohydride (NaBH$_4$), 2-(methoxy)ethyl-amine, 2-pyridinecarboxaldehyde, 2-acetylpyridine, N,N-(diethyl)ethylenediamine and ethanolamine were obtained from Sigma-Aldrich and used as received. ^{1}H NMR and ^{13}C {^{1}H} NMR spectra were recorded on a Bruker 400 MHz spectrometer in CDCl$_3$ solution at room temperature using tetramethylsilane as an internal standard. Elemental analyses were performed

on a Thermal Scientific Flash 2000 while ESI-mass spectra were recorded on an LC premier micro-mass spectrometer. The infrared spectra were recorded on a Perkin-Elmer Spectrum 100 in the 4000-650cm^{-1} range. Magnetic moments of the complexes were determined using Evans balance. GC analyses were performed using a Varian CP-3800 gas chromatograph equipped with a CP-Sil 5 CB (30 m $\times$ 0.2 mm $\times$ 0.25 µm) capillary column while GC‑MS analyses were performed on a Shimadzu GC‑MS-QP2010.

Syntheses of (amino)pyridine ligands and their nickel(II) metal complexes

*N-(2-methoxyethyl)-1-(pyridin-2-yl)ethanamine (**L1a**)*

To a methanol solution of 2-methoxy-N-(1-(pyridin-2-yl)ethylidene)ethanamine (0.5 g, 2.80 mmol) was added NaBH$_4$ (0.53 g, 14.03 mmol) and stirred at 25 °C for 4 h. The brown solution of 2-methoxy-N-(1-(pyridin-2-yl)ethylidene)ethanamine changed to light orange during this period. The solvent was evaporated and the resulting liquid was then re-dissolved in CHCl$_3$ and washed once with 20 mL of deionised water. The organic layer was dried over anhydrous MgSO$_4$ and reduced under vacuum to afford **L1a** as light orange oil. Yield = 0.42 g (83%). ^{1}H NMR (400 MHz, CDCl$_3$): δ 1.39 (d, 3H, $^3J_{HH}$ = 6.8 Hz, CH$_3$); 2.59 (t, 1H, $^3J_{HH}$ = 6.0 Hz, CH$_2$-NH); 2.69 (t, 1H, $^3J_{HH}$ = 6.0 Hz, CH$_2$-NH); 3.34 (s, 3H, CH$_3$-O); 3.45 (t, 1H, $^3J_{HH}$ = 6.0 Hz, CH$_2$-O); 3.60 (t, 1H, $^3J_{HH}$ = 6.0 Hz, CH$_2$-O); 3.87 (q, 1H, $^3J_{HH}$ = 6.8 Hz, CH-NH); 7.33 (d, 1H, $^3J_{HH}$ = 7.6 Hz, 3-py-H); 7.62 (m, 2H, $^3J_{HH}$ = 7.6 Hz, 4,5-py-H); 8.54 (d, 1H, $^3J_{HH}$ = 7.6 Hz, 6-py-H). ^{13}C{^{1}H} NMR (CDCl$_3$): δ 17.18 (CH$_3$-C), 46.57 (CH$_2$-N), 58.65 (CH$_3$-O), 60.28 (CH-N), 71.79 (CH$_2$-N), 121.51 (3-py), 124.34 (5-py), 136.68 (4-py), 149.19 (6-py), 163.32 (2-py). FT-IR (cm^{-1}): 3313 υ(NH). Anal. Calcd for C$_{10}$H$_{16}$N$_2$O·0.25CHCl$_3$: C, 58.60; H, 7.80; N, 13.33. Found: C, 58.78; H, 7.71; N, 13.41.

Compounds **L2a, L3a** and **L4a** were prepared following the same procedure as described for compound **L1a**, using the appropriate reagents.

*2-methoxy-N-((pyridin-2-yl)methyl)ethanamine (**L2a**)*

2-methoxy-N-((pyridin-2-yl)methylene)ethanamine (0.50 g, 3.05 mmol) was reacted with NaBH$_4$ (0.58 g, 15.24 mmol) to give a light orange oil. Yield = 0.44 g (87%). ^{1}H NMR (400 MHz, CDCl$_3$): δ 2.82 (t, 2H, $^3J_{HH}$ = 5.6 Hz, CH$_2$-NH); 3.34 (s, 3H, CH$_3$-O); 3.51 (t, 2H, $^3J_{HH}$ = 5.6 Hz, CH$_2$-O); 3.93 (s, 2H, CH$_2$-py); 7.12 (dd, 1H, $^3J_{HH}$ = 8.0 Hz, 4-py-H); 7.30 (d, 1H, $^3J_{HH}$ = 8.0 Hz, 6-py-H); 7.60 (dd, 1H, $^3J_{HH}$ = 8.0 Hz, 5-py-H); 8.53 (d, 1H, $^3J_{HH}$ = 8.0 Hz, 3-py-H).^{13}C{^{1}H} NMR (CDCl$_3$): δ 48.68 (CH$_2$-N), 54.67 (CH$_2$-py), 58.79 (CH$_3$-O), 71.54 (CH$_2$-O), 121.11 (5-py), 122.33 (3-py), 136.57 (4-py), 149.27 (6-py), 158.73 (2-py). FT-IR (cm^{-1}): 3366 υ(NH).ESI-MS: m/z (%) 167 [M$^+$, 100%]; 189 [(M + Na)$^+$, 55%]. Anal. Calcd for C$_9$H$_{14}$N$_2$O: C, 65.03; H, 8.49; N, 16.85. Found: C, 65.46; H, 8.06; N, 16.52.

*N,N-diethyl-N-((pyridin-2-yl)methyl)ethane-1,2-diamine (**L3a**)*

N,N-diethyl-N-((pyridin-2-yl)methylene)ethane-1,2-diamine (0.50 g, 2.44 mmol) was reacted with NaBH$_4$ (0.46 g, 12.18 mmol) to give a light orange oil. Yield = 0.47 g (94%).^{1}H NMR (400 MHz, CDCl$_3$): δ 0.98 (t, 6H, $^3J_{HH}$ = 7.2 Hz, CH$_3$-Et$_2$); 2.48 (q, 4H, $^3J_{HH}$ = 7.2 Hz, CH$_2$-Et$_2$); 2.57 (t, 2H, $^3J_{HH}$ = 6.4 Hz, CH$_2$-NH); 2.69 (t, 2H, $^3J_{HH}$ = 6.4 Hz, CH$_2$-N); 3.92 (s, 2H, CH$_2$-py); 6.20 (d, 1H, $^3J_{HH}$ = 8.0 Hz, 6-py-H); 7.30 (d, 1H, $^3J_{HH}$ = 8.0 Hz, 3-py-H); 7.60 (dd, 1H, $^3J_{HH}$ = 8.0 Hz, 4-py-H); 8.53 (dd, 1H, $^3J_{HH}$ = 8.0 Hz, 5-py-H).^{13}C{^{1}H} NMR (CDCl$_3$): δ 11.58 (CH$_3$-Et$_2$), 46.13 (CH$_2$-NH), 47.05 (CH$_2$-Et$_2$), 52.56 (CH$_2$-N), 55.16 (CH$_2$-py), 121.86 (3-py), 122.17 (5-py), 136.39 (4-py), 149.22 (6-py), 159.76 (2-py). FT-IR (cm^{-1}): 3304. υ(NH). ESI-MS:

m/z (%) 208 [M$^+$, 100%]; 230 [(M + Na)$^+$, 81%]. Anal. Calcd for C$_{12}$H$_{21}$N$_3$· 0.5CHCl$_3$: C, 56.23; H, 8.12; N, 15.74. Found: C, 55.96; H, 7.66; N, 15.27.

*2-((pyridin-2-yl)methylamino)ethanol (**L4a**)*

2-((pyridin-2-yl)methyleneamino)ethanol (0.50 g, 3.33 mmol) was reacted with NaBH$_4$ (0.63 g, 16.65 mmol) to give a light brown oil. Yield = 0.44 g (87%). ^{1}H NMR (400 MHz, CDCl$_3$): δ 2.76 (t, 2H, ^{3}J$_{HH}$ = 5.4 Hz, CH$_2$-NH); 3.62 (t, 2H, ^{3}J$_{HH}$ = 5.4 Hz, CH$_2$-O); 3.88 (s, 2H, CH$_2$-py); 7.11 (dd, 1H, ^{3}J$_{HH}$ = 7.6 Hz, 4-py-H); 7.24 (d, 1H, ^{3}J$_{HH}$ = 7.6 Hz, 6-py-H); 7.59 (dd, 1H, ^{3}J$_{HH}$ = 7.6 Hz, 5-py-H); 8.48 (d, 1H, ^{3}J$_{HH}$ = 7.6 Hz, 3-py-H). ^{13}C{^{1}H} NMR (CDCl$_3$): δ 51.07 (CH$_2$-NH), 54.35 (CH$_2$-py), 60.73 (CH$_2$-O), 122.11 (5-py), 122.48 (3-py), 136.72 (4-py), 149.05 (6-py), 159.30 (2-py). FT-IR (cm^{-1}): 3278. υ(NH) ESI-MS: m/z (%) 153 [M$^+$, 100%]; 175 [(M + Na)$^+$, 27%]. Anal. Calcd for C$_8$H$_{12}$N$_2$O: C, 63.13; H, 7.95; N, 18.41. Found: C, 62.88; H, 7.49; N, 18.07.

*Bis{2-methoxyethyl-1-(pyridin-2-yl)ethanamine}1NiBr$_2$ (**1**)*

A THF solution (5 mL) of **L1a** (0.10 g, 0.55 mmol) was added to a THF solution (5 mL) of [NiBr$_2$DME] (0.17 g, 0.55 mmol). The reaction mixture turned dark brown immediately and was allowed to stir for 24 h. The resultant precipitate was then isolated by filtration, washed with diethyl ether to afford complex **1** as a brown solid. Yield = 0.17 g (76%). FT-IR (cm^{-1}): 3402 υ(NH). ESI-MS: m/z (%) 317 [(M-Br)$^+$, 100%]. μ$_{eff}$ = 3.72 BM. Calcd for C$_{20}$H$_{32}$Br$_2$N$_4$NiO$_2$·4H$_2$O: C, 36.90; H, 6.19; N, 8.61. Found: C, 37.01; H, 5.92; N, 8.64.

Complexes **2**-**4** were prepared following the procedure described for complex **1**.

Bis{2-methoxy-N-((pyridin-2-yl)methyl)ethanamine}NiBr$_2$] (2)

[NiBr$_2$DME] (0.19 g, 0.60 mmol) and **L2a** (0.10 g, 0.60 mmol). Green solid was formed which on recrystallization from CHCl$_3$ solution afforded green crystals suitable for single-crystal X-ray analysis. Yield: 0.17 g (75%). FT-IR (cm^{-1}): 3238. υ(NH). ESI-MS: m/z (%) 304 [(M-Br)$^+$, 100%]. μ$_{eff}$ = 3.77 BM. Calcd for C$_{18}$H$_{28}$Br$_2$N$_4$NiO$_2$: C, 39.24; H, 5.12; N, 10.17. Found: C, 39.57; H, 5.65; N, 10.53.

Bis{N,N-diethyl-N-((pyridin-2-yl)methyl)ethane-1,2-diamine}NiBr$_2$ (3)

[NiBr$_2$DME] (0.15 g, 0.48 mmol) and **L3a** (0.10 g, 0.48 mmol). Green solid. Yield: 0.16 g (79%). FT-IR (cm^{-1}): 3393. υ(NH). ESI-MS: m/z (%) 346 [(M-Br)$^+$, 25%]; 264 [(M-Br$_2$)$^+$, 100%]. μ$_{eff}$ = 3.70 BM. Calcd for C$_{24}$H$_{42}$Br$_2$N$_6$Ni: C, 42.82; H, 5.75; N, 12.48. Found: C, 43.13; H, 6.22; N, 12.86.

Bis{2-((pyridin-2-yl)methylamino)ethanol}NiBr$_2$ (4)

[NiBr$_2$DME] (0.20 g, 0.66 mmol) and **L4a** (0.10 g, 0.66 mmol). Violet solid was formed which on recrystallization from CHCl$_3$ solution afforded violet crystals suitable for single-crystal X-ray analysis. Yield: 0.20 g (83%). FT-IR (cm^{-1}): 3069. υ(NH). ESI-MS: m/z (%) 290 [(M-Br)$^+$, 49%]; 209 [(M-Br$_2$)$^+$, 27%]. μ$_{eff}$ = 3.75 BM. Calcd for C$_{16}$H$_{24}$Br$_2$N$_4$NiO$_2$·2H$_2$O: C, 34.38; H, 5.05; N, 10.02. Found: C, 34.41; H, 4.58; N, 10.02.

X-ray crystallography

X-ray data collection for compounds **2** and **4** were recorded on a Bruker Apex Duo equipped with an Oxford Instruments Cryojet operating at 100(2) K and an Incoatec microsource operating at 30 W power. Crystal and structure refinement data are given in Table 1. The data

were collected with Mo Kα (λ = 0.71073 Å) radiation at a crystal-to-detector distance of 50 mm. The following conditions were used for the data collection: omega and phi scans with exposures taken at 30 W X-ray power and 0.50° frame widths using APEX2.[56] The data were reduced with the programme SAINT[56] using outlier rejection, scan speed scaling, as well as standard Lorentz and polarisation correction factors. A SADABS semi-empirical multi-scan absorption correction[56] was applied to the data. Direct methods, SHELXS-2014[57] and WinGX[58] were used to solve both structures. All non-hydrogen atoms were located in the difference density map and refined anisotropically with SHELXL-2014.[57] All hydrogen atoms were included as idealized contributors in the least squares process. Their positions were calculated using a standard riding model with C–H$_{aromatic}$ distances of 0.93 Å and U_{iso} = 1.2 U_{eq} and C–H$_{methylene}$ distances of 0.99 Å and U_{iso} = 1.2 Ueqand C–H$_{methyl}$ distances of 0.98 Å and U_{iso} = 1.5 Ueq. The amine N-H and hydroxyl O–H and water hydrogen atoms were located in the difference density map and refined isotropically.

General procedure for ethylene oligomerization reactions

Ethylene oligomerization reactions were carried out in a 400 mL stainless steel Parr reactor equipped with a mechanical stirrer, temperature controller and an internal cooling system. In a typical experiment, the reactor was preheated to 100 ºC in *vacuo* and cooled to room temperature. An appropriate amount of the catalyst precursor (10.0 µmol) was transferred into a dry Schlenk tube under nitrogen and toluene (20 mL) was added using a syringe. The required amount of co-catalyst (EtAlCl$_2$ or MAO) was then injected into the Schlenk tube containing the pre-catalyst, and the resultant solution was transferred *via* cannula into the reactor. An additional 60 mL of toluene solvent was also transferred *via* cannula into the reactor giving a total volume

of 80 mL. The reactor was then flushed three times with ethylene and the desired pressure and

temperature was set and the reaction started. After the reaction time, the reaction was stopped by

cooling the reactor to -20 °C and excess ethylene vented off. An exact amount of heptane (0.1

mL) was added as an internal standard and the mixture was analyzed quantitatively by GC.

Density functional theoretical (DFT) studies

DFT calculations were performed in gas phase to identify the energy-minimized

structures based on B3LYP/LANL2DZ.[59-61] The Gaussian09 suite of programs was used for all

the computations.[62] The geometries and energies of the complexes were optimized using a split

basis set; LANL2DZ for Pd and 6-311G for all other atoms. The structures of the complexes

were optimized without symmetry constraints.
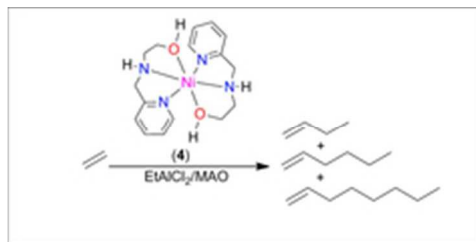
References

1.   J. Ye, B. Jiang, J. Wang, Y. Yang and Q. Pu, *J. Polym. Sci. Part A: Polym. Chem.*, 2014, **52**, 2748-2759.

2.   P.-A. R. Breuil, L. Magna and H. Olivier-Bourbigou, *Catal. Lett.*, 2015, **145**, 173-192.

3.   G. J. Britovsek, D. S. McGuinness, T. Wierenga and C. Young, *ACS Catalysis*, 2015.

4.   A. Forestière, H. Olivier-Bourbigou and L. Saussine, *Oil Gas Sci. Technol.*, 2009, **64**, 649-667.

5.   D. Vogt, in *Applied Homogeneous Catalysis with Organometallic Compounds*, ed. B. C. a. W. A. Herrmann, WILEY-VCH, New York, 1996, vol. 2, ch. 2, pp. 240-252.

6.   W. Keim, F. H. Kowaldt, R. Goddard and C. Krüger, *Angew. Chem. Int. Ed.*, 1978, **17**, 466-467.

7.   J. Skupinska, *Chem. Rev.*, 1991, **91**, 613-648.

8.   G. Mao, Y. Jiang, N. Li, Q. Wang, D. Zheng, M. Li and Y. Ning, *Chin. Sci. Bull.*, 2014, **59**, 2505-2512.

9.   S. P. Netalkar, S. Budagumpi, H. H. Abdallah, P. P. Netalkar and V. K. Revankar, *J. Mol. Struct.*, 2014, **1075**, 559-565.

10.   Y. Imanishi and N. Naga, *Progr. Polym. Sci.*, 2001, **26**, 1147-1198.

11.   D. P. Gates, S. A. Svejda, E. Oñate, C. M. Killian, L. K. Johnson, P. S. White and M. Brookhart, *Macromolecules*, 2000, **33**, 2320-2334.

12.   L. K. Johnson, C. M. Killian and M. Brookhart, *J. Am. Chem. Soc.*, 1995, **117**, 6414-6415.

13.   C. M. Killian, L. K. Johnson and M. Brookhart, *Organometallics*, 1997, **16**, 2005-2007.

14.   X. Tang, W.-H. Sun, T. Gao, J. Hou, J. Chen and W. Chen, *J.Organomet. Chem.*, 2005, **690**, 1570-1580.

15.   S. Kinoshita, K. Kawamura and T. Fujita, *Chem. Asian J*, 2011, **6**, 284-290.

16.   S. Wang, W.-H. Sun and C. Redshaw, *J. Organomet. Chem.*, 2014, **751**, 717-741.

17.   N. Fey, J. N. Harvey, G. C. Lloyd-Jones, P. Murray, A. G. Orpen, R. Osborne and M. Purdie, *Organometallics*, 2008, **27**, 1372-1383.

18.   B. L. Small, *Acc. Chem. Res.*, 2015, **48**, 2599-2611.

19.   G. S. Nyamato, S. O. Ojwach and M. P. Akerman, *Organometallics*, 2015, **34**, 5647-5657.

20.   M. K. Ainooson, I. A. Guzei, L. C. Spencer and J. Darkwa, *Polyhedron*, 2013, **53**, 295-303.

21.   C. Obuah, B. Omondi, K. Nozaki and J. Darkwa, *J. Mol. Catal. A: Chem.*, 2014, **382**, 31-40.

22.   N. Colthup, *Introduction to infrared and Raman spectroscopy*, Elsevier, 2012.

23.   A. F. Cotton, G. Wilkinson, M. Bochmann and C. A. Murillo, *Advanced inorganic chemistry*, Wiley, 1999.

24.   T.-L. Ho, *Hard and soft acids and bases principle in organic chemistry*, Elsevier, 2012.

25.   M. P. Akerman and V. A. Chiazzari, *J. Mol. Struct.*, 2014, **1058**, 22-30.

26.   A. Ghisolfi, C. Fliedel, V. Rosa, K. Y. Monakhov and P. Braunstein, *Organometallics*, 2014, **33**, 2523-2534.

27.   J. Flapper, P. W. van Leeuwen, C. J. Elsevier and P. C. Kamer, *Organometallics*, 2009, **28**, 3264-3271.

28. M. K. Ainooson, S. O. Ojwach, I. A. Guzei, L. C. Spencer and J. Darkwa, *J. Organomet. Chem.*, 2011, **696**, 1528-1535.

29. A. Budhai, B. Omondi, S. O. Ojwach, C. Obuah, E. Y. Osei-Twum and J. Darkwa, *Catal. Sci. Technol.*, 2013, **3**, 3130-3135.

30. G. S. Nyamato, S. O. Ojwach and M. P. Akerman, *J. Mol. Catal. A: Chem.*, 2014, **394**, 274-282.

31. S. O. Ojwach, I. A. Guzei, L. L. Benade, S. F. Mapolie and J. Darkwa, *Organometallics*, 2009, **28**, 2127-2133.

32. G. S. Nyamato, M. G. Alam, S. O. Ojwach and M. P. Akerman, *J. Organomet. Chem.*, 2015, **783**, 64-72.

33. S. Song, Y. Li, C. Redshaw, F. Wang and W.-H. Sun, *J.Organomet. Chem.*, 2011, **696**, 3772-3778.

34. P. Chavez, I. G. Rios, A. Kermagoret, R. Pattacini, A. Meli, C. Bianchini, G. Giambastiani and P. Braunstein, *Organometallics*, 2009, 28, 1776-1784.

35. A. J. Swarts and S. F. Mapolie, *Dalton Trans.*, 2014, **43**, 9892-9900.

36. S. Dagorne, C. Aiedel, S. Woodward, S. Dagorne, *Top. Organomet. Chem*. 2013, 41, 125-172.

37. Z. J. Komon, X. Bu and G. C. Bazan, *J. Am. Chem. Soc.*, 2000, **122**, 12379-12380.

38. J. S. Rogers, X. Bu and G. C. Bazan, *Organometallics*, 2000, **19**, 3948-3956.

39. N. Ajellal, M. C. Kuhn, A. D. Boff, M. Hörner, C. M. Thomas, J.-F. Carpentier and O. L. Casagrande, *Organometallics*, 2006, **25**, 1213-1216.

40. L. L. de Oliveira, R. R. Campedelli, M. C. Kuhn, J.-F. Carpentier and O. L. Casagrande, *J. Mol. Catal. A: Chem.*, 2008, **288**, 58-62.

41. K. Song, H. Gao, F. Liu, J. Pan, L. Guo, S. Zai and Q. Wu, *Eur. J. Inorg. Chem.*, 2009, **2009**, 3016-3024.

42. A. J. Swarts, F. Zheng, V. J. Smith, E. Nordlander and S. F. Mapolie, *Organometallics*, 2014, **33**, 2247-2256.

43. B. Milani, A. Marson, A. Scarel, G. Mestroni, J. M. Ernsting and C. J. Elsevier, *Organometallics*, 2004, **23**, 1974-1977.

44. K. Ohno, A. Nagasawa and T. Fujihara, *Dalton Trans.*, 2015, **44**, 368-376.

45.   A. Boudier, P.-A. R. Breuil, L. Magna, H. Olivier-Bourbigou and P. Braunstein, *J. Organomet. Chem.*, 2012, **718**, 31-37.

46.   W. Chai, J. Yu, L. Wang, X. Hu, C. Redshaw and W.-H. Sun, *Inorg. Chim. Acta*, 2012, **385**, 21-26.

47.   Q.-s. Shi, X. Hao and C. Redshaw, *Chin. J. Polym. Sci.*, 2013, **31**, 769-777.

48.   A. H. Ulbrich, R. R. Campedelli, J. L. S. Milani, J. H. dos Santos and O. d. L. Casagrande, *Appl. Catal. A: Gen.*, 2013, **453**, 280-286.

49.   S. Liu, Y. Zhang, Q. Huo, S. He and Y. Han, *J. Spectrosc.*, 2014, **2014**.

50.   K. R. Birdwhistell and J. Lanza, *J. Chem. Educ.*, 1997, **74**, 579.

51.   F. Speiser, P. Braunstein and L. Saussine, *Organometallics*, 2004, **23**, 2633-2640.

52.   X. Tang, D. Zhang, S. Jie, W.-H. Sun and J. Chen, *J. Organomet. Chem.*, 2005, **690**, 3918-3928.

53.   B. L. Small and M. Brookhart, *J. Am. Chem. Soc.*, 1998, **120**, 7143-7144.

54.   W. Yang, J. Yi and W. H. Sun, *Macromol. Chem. Phys.*, 2015, **216**, 1125-1133.

55.   P. Huo, W. Liu, X. He, H. Wang and Y. Chen, *Organometallics*, 2013, **32**, 2291-2299.

56.   Bruker,APEX2, SAINT and SADABS. Bruker AXS Inc., Madison, Wisconsin, USA, 2012.

57.   G. M. Sheldrick, *Acta Crystallogr. Sect. A: Found. Crystallogr.*, 2007, **64**, 112-122.

58.   L. J. Farrugia, *Appl. Crystallogr.*, 2012, **45**, 849-854.

59.   P. J. Hay and W. R. Wadt, *J. Chem. Phys.*, 1985, **82**, 270-283.

60.   A. D. Becke, *J. Chem. Phys.*, 1993, **98**, 5648-5652.

61.   C. Lee, W. Yang and R. G. Parr, *Phys. Rev. B*, 1988, **37**, 785-789.

62.   M. J. T. Frisch, G. W.; Schlegel, H. B.; Scuseria, G. E.; Robb, M. A.; Cheeseman, J. R.; Scalmani, G.; Barone, V.; Mennucci, B.; Petersson, G. A.; Nakatsuji, H.; Caricato, M.; Li, X.; Hratchian, H. P.; Izmaylov, A. F.; Bloino, J.; Zheng, G.; Sonnenberg, J. L.; Hada, M.; Ehara, M.; Toyota, K.; Fukuda, R.; Hasegawa, J.; Ishida, M.; Nakajima, T.; Honda, Y.; Kitao, O.; Nakai, H.; Vreven, T.; Montgomery Jr., J. A.; Peralta, J. E.; Ogliaro, F.; Bearpark, M.; Heyd, J. J.; Brothers, E.; Kudin, K. N.; Staroverov, V. N.; Kobayashi, R.; Normand, J.; Raghavachari, K.; Rendell, A.; Burant, J. C.; Iyengar, S. S.; Tomasi, J.; Cossi, M.; Rega, N.; Millam, J. M.; Klene, M.; Knox, J. E.; Cross, J. B.; Bakken, V.; Adamo, C.; Jaramillo, J.; Gomperts, R.; Stratmann, R. E.; Yazyev, O.; Austin, A. J.;

30

Cammi, R.; Pomelli, C.; Ochterski, J. W.; Martin, R. L.; Morokuma, K.; Zakrzewski, V. G.; Voth, G. A.; Salvador, P.; Dannenberg, J. J.; Dapprich, S.; Daniels, A. D.; Farkas, O.; Foresman, J. B.; Ortiz, J. V.; Cioslowski, J.; Fox, D. J., *GAUSSIAN 09 (Revision A.1), Gaussian, Inc., Wallingford CT, 2009.*

20x10mm (300 x 300 DPI)